Contact Aggregation, Bridging, and Steric Stabilization in Dense Polymer−Particle Mixtures

Justin B. Hooper and Kenneth S. Schweizer*

Department of Materials Science and Engineering and Frederick Seitz Materials Research Laboratory, University of Illinois, 1304 West Green Street, Urbana, Illinois 61801

Received June 21, 2005

ABSTRACT: A detailed computational study of the potential of mean force between a pair of spherical particles dissolved in a homopolymer melt has been performed using microscopic liquid state theory. The role of particle-to-monomer diameter ratio, degree of polymerization, strength and spatial range of monomer−particle attractions, and direct interfiller attractions has been established. Beyond the small particle regime, the potential of mean force scales linearly with the particle-to-monomer diameter ratio. This simple scaling allows the construction of master curves and the quantification of material specific aspects independent of the filler-to-monomer diameter ratio. For hard-sphere fillers, four general categories of polymer-mediated organization are found: contact aggregation due to depletion attraction, segment level tight particle bridging, steric stabilization due to thermodynamically stable "bound polymer layers", and "tele-bridging" where distinct adsorbed layers coexist with longer range bridging. The conditions on the strength and spatial range of monomer−particle attractive interactions that define these different modes of organization have been established. Direct interparticle van der Waals attractions favor contact aggregation and thus compete with the rich polymer-mediated behavior. As the direct attractions increase in strength, the globally stable noncontact bridging configuration is gradually destabilized and replaced by contact aggregation as the most favored state of packing. However, bridging states often remain as metastable local minima. Steric stabilization systems are much less affected by direct interfiller attractions due to the thermodynamic stability of distinct bound polymer layers. This suggests design rules for achieving good particle dispersion. In addition, the interesting possibility is raised that sterically stabilized nanofillers may crystallize in a homopolymer matrix at relatively low volume fractions. Our results have implications for nonequilibrium phenomena such as gelation or filler network formation and kinetic stabilization via large repulsive barriers, which are qualitatively discussed.

I. Introduction

Mixtures of polymers and spherical particles are of major scientific and technological interest in diverse areas of colloid science,[1−4] polymer science,[5−8] nanomaterials,[9−11] and biology.[12] Structural and phase behavior complexity arises due to the competition between the ideal and excess entropic effects associated with species of different size, geometry and/or conformation, and the enthalpic consequences of intermolecular, often attractive, interactions.[1−3] Experience in the field of colloidal suspensions has shown the physical behavior is very sensitive to the strength and spatial range of direct and induced attractive interactions. For example, entropy-controlled suspensions of hard-sphere colloids and nonadsorbing polymers can exist as homogeneous fluids, macroscopically phase separate, crystallize, or form nonequilibrium gels depending on the size and concentration of polymers.[2−4] If monomers are even weakly attracted to particle surfaces, then more complexity emerges since now polymers can also induce steric stabilization (discrete bound layers which repel in a good solvent), bridging attraction (tight or loose) where polymer is shared between particles and a network type structure emerges, and/or contact depletion aggregation. Both enthalpy and entropy are important. In charged or sterically stabilized colloidal suspensions, crystals can form at low physical volume fractions with a lattice symmetry that depends on the range or softness of the effective intermolecular repulsions.[1] Direct van der Waals attractions can also induce crystallization, phase separation, or physical gelation.[1,13]

Our present interest is dense polymer−particle mixtures, or polymer nanocomposites (PNC), for which there has been far less systematic exploration of the complex physics sketched above for suspensions. Besides its intrinsic scientific interest, understanding these issues may allow the design of new polymer nanocomposite materials of technological importance.[5−11] Fundamental issues include equilibrium miscibility, dispersion and spatial organization of particles or fillers, particle-induced modification of polymer conformation and packing, structure of the polymer−particle interface, and the consequences of all these considerations on thermomechanical properties.

Diverse theoretical and simulation approaches have begun to be employed to study elementary aspects of model polymer−particle mixtures.[14−27] Classic self-consistent mean-field theory and scaling arguments have been applied to compute depletion forces between large colloids immersed in semidilute polymer solutions.[28−31] Various density functional theory (DFT) and "wall integral equation" studies of dense polymer fluids confined between flat surfaces, or in the presence of spherical nanoparticles, have been pursued.[14−16] Most work has focused on the two particle problem and potential of mean force, often for athermal models where entropic excluded-volume effects are dominant.

Very recently, we have employed the microscopic polymer reference interaction site model (PRISM) integral equation theory[32] to investigate structure, effective forces, and thermodynamics in dense, *athermal*

* Corresponding author. E-mail: kschweiz@uiuc.edu.

10.1021/ma051318k CCC: $30.25
Published on Web 09/13/2005

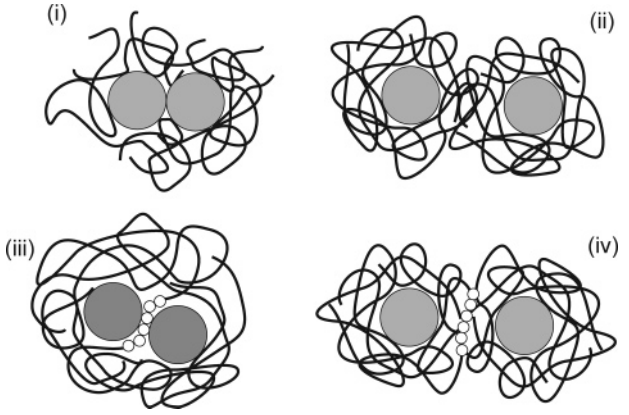

Figure 1. Schematic illustration of four states of particle organization in a dense polymer melt: (i) direct contact aggregation due to depletion attraction, (ii) steric stabilization with noninterpentrating adsorbed polymer layers, (iii) segment level tight particle bridging, and (iv) "tele-bridging" where distinct adsorbed layers coexist with longer range bridging.

polymer−particle mixtures in the one- and two-particle limit.[17] The influence of particle size, degree of polymerization, and polymer reduced density has been established. Oscillatory depletion forces between two hard spheres occur under melt conditions due to monomer level packing correlations. The potential of mean force generally exhibits extremely large attractive interactions at contact. The polymer radius of gyration, R_g, is not the key variable, but rather the ratio of particle diameter to monomer diameter, D/d, is crucial. The range of oscillatory depletion forces in athermal mixtures is controlled by the intrinsic density fluctuation correlation length of the dense polymer fluid which is typically a few monomer diameters.[33] By comparing the theoretical results with complementary molecular dynamics simulations, PRISM with the hypernetted chain closure[34,35] for particle−particle direct correlations has been shown to capture all the rich features found in the simulations, with quantitative errors for the amplitude of depletion forces at the level of a factor of 2 or less.[17]

The presence of strong polymer-mediated attractions between particles at contact suggests purely athermal mixtures are macroscopically phase separated in equilibrium. Hence, as long appreciated in the practical filled polymer composite field,[5,8] attractive interactions between polymer and particle are required to achieve some degree of miscibility or dispersion. The goal of the present paper is to explore this issue in depth at the two particle potential of mean force level. The often competing consequences of direct (van der Waals) particle−particle attractions and monomer−particle attractions are studied. Both the strength and spatial range of intermolecular attractions are important and can potentially be tuned via material chemistry (e.g., H-bonding vs dispersion attractions).

The primary message of our present work is that the particle−particle potential of mean force, $W_{cc}(r)$, can exhibit multiple qualitatively different behaviors depending on the strength and spatial range of intermolecular attractions. These include (i) contact aggregation, (ii) steric stabilization, (iii) local bridging attraction, or (iv) longer range "tele-bridging" attraction. A schematic of these different states of organization is given in Figure 1. Our goal is to quantify these cartoons and establish the relationship between the state of organization and controllable system parameters including the monomer and filler diameters, polymer degree of polymerization, and detailed nature of the polymer−particle and particle−particle attractive interactions. Of particular interest is identifying "design rules" for thermodynamic stability and miscibility of fillers in dense polymer melts. We find there is a reasonably good "decoupling" of the size asymmetry and intermolecular attraction aspects of the problem, thereby allowing chemical trends associated with variable intermolecular attractions to be established in a nearly size ratio independent manner. Of course, the size asymmetry ratio is important since the absolute magnitude of $W_{cc}(r)$ relative to the thermal energy is found to scale with D/d.

Although our calculations are of an equilibrium nature, they have implications for several ubiquitous nonequilibrium phenomena which we discuss qualitatively. For example, deep enough local minima in $W_{cc}(r)$ can trigger the formation of a particle gel or network of either a contact aggregation or polymer-mediated bridging form.[5,8,18] Alternatively, if large repulsive barriers proceed local attractive minima in $W_{cc}(r)$, then kinetic stabilization may occur. The latter situation is analogous to the classic case of suspensions of sticky charged colloids stabilized by suitably strong and long-range Coulomb repulsions.[1]

The remainder of the paper is structured as follows. In section II we briefly review the version of PRISM theory and chain model utilized and discuss the attractive model potentials employed. Section III studies in depth the case of hard-sphere fillers. The effect of particle−monomer diameter ratio, and strength and spatial range of interfacial attractions, on the filler−filler potential of mean force are systematically explored. The possibility of polymer-mediated crystallization of fillers is briefly discussed. The influence of polymer degree of polymerization on the local and long-range aspects of the interparticle potential of mean force is studied in section IV. The consequence of direct van der Waals attractions between particles is the subject of section V. The paper concludes in section VI with a summary and discussion, including directions for future work.

II. Theory and Model

The version of PRISM theory and specific polymer chain model employed have been described previously.[17] In this section we briefly summarize the required equations. A new comparison of the simple exponential form of polymer−particle attractive interaction employed with a more rigorous colloid science based approach[36] is presented to facilitate interpretation of our model potential parameters in terms of real materials.

A. PRISM Theory and Chain Model. PRISM theory[32] is a generalization to polymers of small molecule RISM theory.[34] By treating all sites on a chain as statistically equivalent, the matrix site−site generalized Ornstein−Zernike equations in Fourier space are given by[32,34]

$$h_{ij}(k) = \omega_i(k)[C_{ij}(k)\,\omega_j(k) + \sum_l C_{il}(k)\rho_l h_{lj}(k)] \quad (1)$$

where $h_{ij}(r) = g_{ij}(r) - 1$ is the nonrandom part of the intermolecular site−site pair correlation function between species i and j, $C_{ij}(r)$ is the corresponding intermolecular direct correlation function, $\omega_i(k)$ is the single

molecule structure factor of species i, and ρ_l is the site number density of species l. Repulsive interactions between all species are modeled as hard-core interactions

$$U_{ij,\mathrm{rep}}(r) = \infty, \quad r \le \sigma_{ij}$$
$$U_{ij,\mathrm{rep}}(r) = 0, \quad r > \sigma_{ij} \tag{2}$$

where σ_{ij} is the distance of closest approach for an additive hard-core potential model. The particle has a diameter $\sigma_{\mathrm{cc}} \equiv D$ and trivial structure factor $\omega_{\mathrm{c}}(k) \equiv 1$. The polymer is modeled as a freely jointed chain (FJC[37]) of N segments with a site diameter $\sigma_{\mathrm{pp}} \equiv d$ and a rigid bond length $l = 4d/3$. The polymer site or monomer diameter is taken as the unit of length throughout the paper. This backbone persistence length of 4/3 is a realistic value for many real flexible polymers[32] and is characteristic of the tangent bead model widely employed in simulation studies.[38] The FJC structure factor is[32,37]

$$\omega_{\mathrm{p}}(k) = (1-f)^{-2}[1 - f^2 - 2N^{-1}f + 2N^{-1}f^{N+1}] \tag{3}$$

where $f \equiv \sin(kl)/kl$. The FJC model ignores nonideal conformational effects, which are expected to be minor for the concentrated and melt conditions of present interest.[17,32,33]

In the infinitely dilute particle limit, $\rho_p d^3$ is the only relevant density, and eq 1 reduces to three uncoupled, sequentially solvable integral equations[3,32,39]

$$h_{\mathrm{pp}}(k) = \omega_{\mathrm{p}}(k)C_{\mathrm{pp}}(k)[\omega_{\mathrm{p}}(k) + \rho_{\mathrm{p}}h_{\mathrm{pp}}(k)] \equiv \omega_{\mathrm{p}}(k)C_{\mathrm{pp}}(k)S_{\mathrm{pp}}(k) \tag{4}$$

$$h_{\mathrm{cp}}(k) = C_{\mathrm{cp}}(k)S_{\mathrm{pp}}(k) \tag{5}$$

$$h_{\mathrm{cc}}(k) = C_{\mathrm{cc}}(k) + \rho_{\mathrm{p}}C_{\mathrm{cp}}{}^2(k)S_{\mathrm{pp}}(k) \tag{6}$$

The pure polymer fluid structure factor is defined in eq 4, and the polymer-mediated potential of mean force between particles is given by

$$W_{\mathrm{cc}}(r) = -k_{\mathrm{B}}T \ln(g_{\mathrm{cc}}(r)) \tag{7}$$

Hard-core interactions imply the exact impenetrability conditions:

$$g_{ij}(r) \equiv 0, \quad r < \sigma_{ij} \tag{8}$$

Closure relations outside the hard core are required. The site−site PY approximation[32,34] is adopted for the polymer−polymer (PP) and polymer−particle (PC) direct correlations

$$C_{ij}(r) = (1 - \mathrm{e}^{\beta U_{ij}(r)})g_{ij}(r), \quad r > \sigma_{ij} \tag{9}$$

where U_{ij} is the total site−site interaction potential. The HNC closure is utilized for the $r > \sigma_{\mathrm{cc}}$ particle−particle (CC) direct correlations[34,35]

$$C_{\mathrm{cc}}(r) = h_{\mathrm{cc}}(r) - \ln g_{\mathrm{cc}}(r) - \beta U_{\mathrm{cc}}(r) \tag{10}$$

The site−site PY closure has been shown to be accurate for pure polymers and polymer−particle correlations under dense melt conditions.[16,32] As discussed previously, use of the HNC closure for particle−particle direct correlations is necessary for the large size asymmetry situation ($D/d \gg 1$) and is quite accurate on the basis of limited comparisons with simulation.[17]

All calculations are performed at a total packing fraction of 0.4, which corresponds to a typical dense melt value with a realistic dimensionless isothermal compressibility.[32] The integral equations are solved numerically using the iterative Picard method.[35]

B. Attractive Potentials. Polymers are treated as athermal hard chains. Given the system specificity of the attractive branch of the true interaction potentials, and our adoption of a coarse-grained polymer model, a minimalist two-parameter monomer−particle attraction of an exponential form is adopted. It is defined by a strength at contact, ϵ_{pc}, and spatial range, αd

$$U_{\mathrm{pc}}(r) = -\epsilon_{\mathrm{pc}} \exp\left[-\frac{r - \sigma_{\mathrm{pc}}}{\alpha d}\right] \tag{11}$$

The strength parameter represents the gain in cohesive energy of a monomer in contact with a particle relative to a monomer−monomer contact. For real systems its magnitude can vary from "weak" (a fraction of a $k_{\mathrm{B}}T$) to strong (several $k_{\mathrm{B}}T$). The spatial range parameter α is also material dependent and, within a coarse-grained chain model, will depend on the angstrom scale chemical details that have been averaged over (e.g., monomer shape). This motivates exploration of the sensitivity of our results to the precise value of α. For a chemically specific type attraction the range can be significantly smaller than the size of a coarse-grained monomer.

To gain insight concerning the appropriate values of α and ϵ_{pc}, we compare eq 11 with the colloid as a composite particle model of Henderson and co-workers[36] which we refer to as the "colloid Lennard-Jones" (CLJ) potential. Two spheres, i and j, of different diameters are each composed of elementary units of size b which interact via a 6−12 Lennard-Jones (LJ) potential with energy parameter E_{ij} (schematically represented in the inset of Figure 2). The net interaction between the two composite spheres is a pairwise sum over LJ potentials holding the interparticle separation fixed at R. The discrete sums are converted to volume integrals corresponding to adopting a continuous distribution of the elementary units[36]

$$U_{ij}(R) = \int u_{\mathrm{LJ}}(r_{ij})\, \mathrm{d}V_i\, \mathrm{d}V_j \tag{12}$$

where $V_i = \pi d_i^3/6$ is the volume of a sphere of type i. In contrast with standard continuum models in colloid science, the inclusion of (and integration over) the repulsive portion of the LJ potential prevents any unphysical divergence of the attractive interactions when the two particles are in contact. Analytic, but very long, expressions for the net interaction potentials $U_{ij}(R)$ have been derived,[36] which we do not reproduce here. Of present interest is the shape, range, and dependence on sphere diameters (b, d, and D) of the *attractive* branch of this potential and what choices of the two parameters of eq 11 mimic it.

The full CLJ potential is a complicated function of all the relevant variables (E_{ij}, d_i, d_j, b). By rearranging the original CLJ potential,[36] we are able to represent the function by the three following terms:

$$U_{ij}(R) \equiv E_{ij}S(d_i,d_j,R)\, m(d_i,d_j) \tag{13}$$

where $S(d_i,d_j,R)$ is normalized to unity at the energy minimum and describes the shape of the attractive

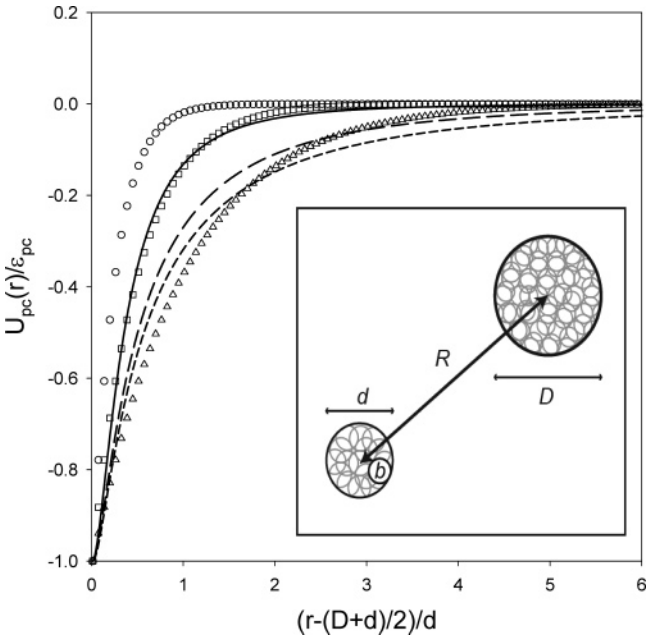

Figure 2. Comparison of normalized attractive potential shapes: exponential potential with $\alpha = 0.25$ (circles), $\alpha = 0.50$ (squares), and $\alpha = 1.00$ (triangles) and the CLJ model[36] with $D/d = 10$ and $d = b$ (solid), $d = 3b$ (long dash), and $d = 6b$ (short dash). The inset shows a schematic of the CLJ model of particles as composite objects.

branch of the potential, and the function $m(d_i,d_j)$ and parameter E_{ij} control the attractive well depth. In the limit of primary interest, d_i, $d_j > b$ and $R > (d_i + d_j)/2$, one has $m \approx fm'$ where $m' \equiv d_i d_j/2b(d_i + d_j)$. Here f is a near unity correction parameter which accounts for the difference between $m'$and m if the particle diameters are not large compared to the elementary length b. The function $S(d_i,d_j,R)$ is given by

$$S(d_i,d_j,R) = \frac{U_{ij}(R)}{E_{ij}fm'} = \frac{U_{ij}(R)}{\epsilon_{ij}} \tag{14}$$

where ϵ_{ij} is the *total* attraction strength at the potential minimum between the two composite spheres

$$\epsilon_{ij} = E_{ij}fm' \tag{15}$$

When applied to the monomer−particle interaction where $d \ll D$ and $m' \approx d/2b$, the attractive minimum energy is

$$\epsilon_{pc} \approx E_{pc}d/2b \tag{16}$$

which is independent of D since the particle appears as a "wall or surface" to the much smaller monomer. For direct particle−particle attractions, $d_i = d_j \equiv D$, $m' = D/4b$, and

$$\epsilon_{cc} \approx E_{cc}D/4b \tag{17}$$

which scales linearly with particle diameter. Note that E_{cc} and E_{pc} are the LJ potential parameters for the elementary units (size b) that compose the monomer and particle. For example, a CH_2 group corresponds to $b \sim 3-4$ Å and $E \sim 40$ K.

To apply these results to our problem requires specification of the size of the elementary unit the monomer and particle are composed of. For the polymer, this is equivalent to making a reasonable guess of what a segment of the freely jointed chain actually is. Consider the following common choice of coarse-graining in polymer physics.[37] The persistence length of a real polymer is $\xi_p = (C_\infty + 1)l_B/2$, where l_B is the mean length of a backbone chemical bond (~1.5 Å) and C_∞ is the characteristic ratio, which is typically ~5−10. Equating this persistence length to its FJC analogue yields an estimate of the site diameter of the FJC model as $d \cong 3l_B(C_\infty + 1)/8 \approx 5 \pm 1$ Å. This corresponds to a site volume of ~30−100 Å^3, values typical of the monomer volumes of many hydrocarbon polymers.[40] This "mapping" is not unique but does lead to the sensible suggestion that the relevant values of d/b for the coarse-grained monomer are of order unity.

Figure 2 plots the CLJ potential for $D/d = 10$ and $d/b = 1, 3, 6$. The $d = b$ curve corresponds to the limiting case of a single LJ unit interacting with the particle, a monomer model adopted in many theoretical and computer simulation studies. The exponential potential is also plotted for various choices of spatial range to test its ability to mimic the more complex CLJ potential. The exponential model with $\alpha = 0.5$ captures the basic shape and range of the $d = b$ attraction very well. We shall interpret it as a crude but reasonable representation of dispersion interactions between a particle and polymer composed of relatively small monomers. The $\alpha = 0.25$ attraction shows a significantly steeper decay than any of the van der Waals potentials, and hence we interpret it as mimicking a chemically specific attraction such as a hydrogen-bonding or perhaps charge-transfer interaction. The $\alpha = 1.0$ exponential is a softer potential near contact than the CLJ potential for $d/b = 3$, 6 while decaying faster at longer ranges. We interpret it as a reasonable representation of larger monomer cases where the coarse-grained site contains a significant number of elementary units. We find that the $\alpha = 1.0$ exponential agrees well with the $d = 15b$ CLJ potential near contact (not shown). With this motiviation, most of our calculations based on eq 11 have been performed for the three representative values of $\alpha = 0.25$, 0.5, and 1.

III. Hard-Sphere Fillers

In this section we consider hard-sphere fillers. The role of variable polymer−particle attractive interactions, particle−monomer size ratio, and degree of polymerization are systematically investigated. Unless stated otherwise, the chain length is $N = 100$. As discussed below, most of the results are rather insensitive to N. All energies are in units of k_BT, and lengths in units of the FJC monomer diameter, d. Interparticle distances are generally discussed in terms of the reduced filler surface-to-surface separation, $(r - D)/d$.

A. Consequences of Interfacial Attraction: Steric Stabilization vs Bridging. To elucidate the general trends and subtle competition between steric stabilization and bridging, we first present calculations for a single particle to monomer diameter ratio of $D/d = 16$. The results are representative of a wide range of size ratios above an extreme nanoparticle limit of $D/d \sim 4-6$. Figure 3 shows the effect of varying the spatial range and strength, α and ϵ_{pc}, of the interfacial attraction on the particle−particle radial distribution function. The main panel is for a fixed, moderate monomer−particle attraction of 1 k_BT. For $\alpha = 0.25$ and $\alpha = 0.5$ highly ordered local packing is found with a single large

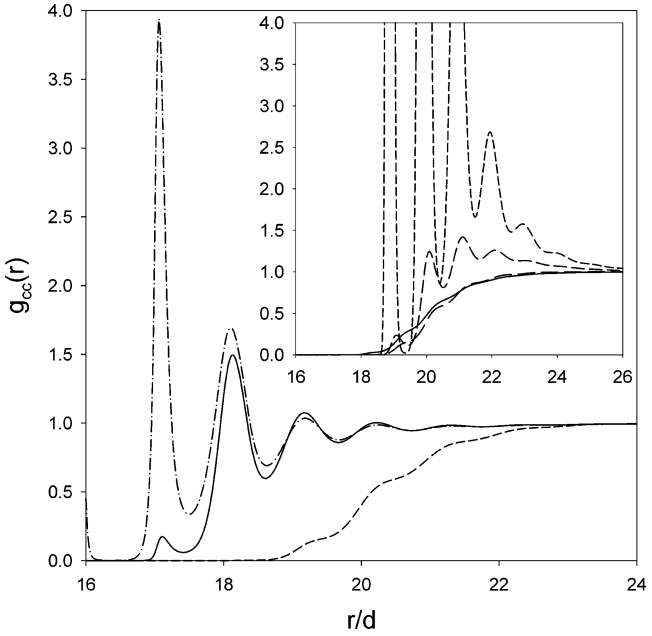

Figure 3. Particle−particle radial distribution function for $D/d = 16$, $\epsilon_{pc} = 1.0$, and $\alpha = 0.25$ (dash−dot), $\alpha = 0.50$ (solid), and $\alpha = 1.00$ (dashed). The inset shows the variation of pair correlation function for $D/d = 16$ and $\alpha = 1.0$ as a function of increasing polymer−particle attraction: $\epsilon_{pc} = 0.5$ (solid), $\epsilon_{pc} = 1.0$ (long dash), $\epsilon_{pc} = 2.0$ (medium dash), and $\epsilon_{pc} = 3.0$ (short dash).

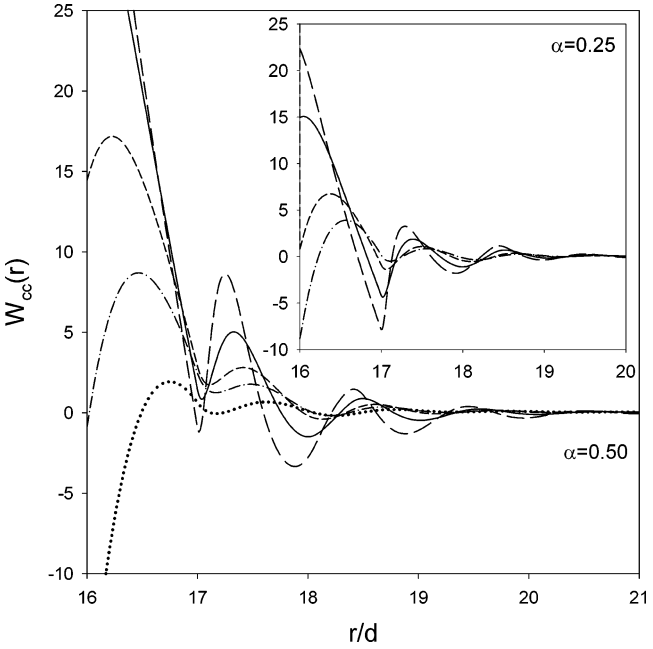

Figure 4. Potentials of mean force for $D/d = 16$ and $\alpha = 0.50$ ($\alpha = 0.25$) are shown in the main graph (inset) for $\epsilon_{pc} = 0.5$ (dash−dot), $\epsilon_{pc} = 1.0$ (short dash), $\epsilon_{pc} = 2.0$ (solid), and $\epsilon_{pc} = 3.0$ (long dash). The PMF of the corresponding athermal system is shown for comparison on the main graph (dotted).

dominant peak at a noncontact interparticle separation. The pair correlation function is oscillatory, approaching the random value of unity at a surface-to-surface separation of ∼4−6d. These are examples of the (tight) "bridging" type of organization which can occur even for moderate values of ϵ_{pc}. The relative height and location of the primary peak is a function of α, and the height (but not location) increases with ϵ_{pc}. The behavior is qualitatively different than found for the athermal case[17] ($\epsilon_{pc} = 0$) where the contact configuration is strongly favored, suggesting a fluid−fluid phase separation in strong contrast to the thermal bridging systems. A secondary trend is that the bridging structure is stronger and tighter for the shorter range polymer−particle attraction.

The behavior of the $\alpha = 1.0$ longer range attraction system in Figure 3 is qualitatively different. A dramatic "depletion hole" emerges corresponding to a strong suppression of the ability of particles to approach closer than ∼4−6 monomer diameters. Although there are very weak oscillatory features, there are no well-defined interparticle separations. Moreover, $g_{cc}(r)$ monotonically approaches the random value of unity from below, and hence the radial distribution takes on a "gaslike" soft repulsive sphere form. These are the signatures of the "sterically stabilized" type of organization. Although bound chains interpenetrate, the particles possess distinct, *thermodynamically stable* noninterpenetrating "bound layers" of 2−3 monomers thickness. In contrast to the bridging systems, from additional calculations (not plotted) we find that for moderate ϵ_{pc} the most probable interparticle separation *is* a function of ϵ_{pc}, but the *magnitudes* of the peaks of $g_{cc}(r)$ at these locations are essentially *insensitive* to ϵ_{pc}. As seen from Figure 3, for higher $\epsilon_{pc} > 1$ the $\alpha = 1.0$ systems begin to show a mixed behavior, i.e., features of both bridging and steric stabilization. With increasing ϵ_{pc} a strong initial layer of depleted nanoparticle contacts coexists with bridging-like behavior superimposed on it, beginning roughly at the end of the bound polymer layer. The approach of $g_{cc}(r)$ to its random value is now from above.

The physics underlying the rich behavior in Figure 3 is the competition between the enthalpic drive to maximize polymer−particle contacts and the conflicting desire to maximize local entropy on the segmental scale. Steric stabilization is a compromise state of organization where polymer−particle adsorption occurs, but the near surface adsorbed monomer layers on the two particles retain their individual identity and resist interpenetration or being squeezed out. Ultimately, at high (short) enough polymer−particle attraction strength (range) this state of organization becomes less favorable relative to the more ordered bridging type packing which is more favored cohesively but costs additional entropy.

There is a rather sharp crossover from bridging to steric stabilization behavior as a function of attraction strength and range. The clearest visualization of this, and insight concerning whether one should expect miscibility, phase separation, or perhaps gelation/network formation, comes from examining the particle−particle potential of mean force (PMF) defined in eq 8. The main panel (inset) of Figure 4 shows the PMF for $D/d = 16$ and several $\alpha = 0.5$ ($\alpha = 0.25$) systems. The contact depletion attraction of the athermal system is enormous, $19k_BT$, which favors particle clustering and macrophase separation. However, it is rather easily broken up by "small" values of ϵ_{pc} ($< k_BT$) due to the ability of many monomers to pack against the particle surface and contribute to enthalpic stabilization of the interface. The formation of a secondary minimum in the PMF at a specific (α-dependent) distance is also seen in Figure 4, with the depth increasing with ϵ_{pc} but at a significantly slower rate than the diminishing of the contact depletion attraction. In general, as α decreases, the primary bridging minimum in the PMF deepens, as seen by comparing the $\alpha = 0.25$ and $\alpha = 0.5$ systems in Figure 4. For a monomer−particle attraction of $3k_BT$,

the $\alpha = 0.25$ system has a very deep bridging attraction well ($W_{cc} \approx 8k_BT$) at a separation of roughly 1 monomer diameter. In contrast, the PMF for the $\alpha = 0.5$ system exhibits a bridging well at a larger separation ($\sim 2d$) which is significantly shallower ($W_{cc} \approx 3.5k_BT$) and is surrounded by additional weaker localization wells of nonnegligible magnitude.

Rather large repulsive barriers emerge at high ϵ_{pc} which separate the primary minimum of the PMF from the tighter secondary and/or contact minima. Barriers are due to two effects. (i) When particles are separated by nonintegral multiples of the monomer diameter, the packing of the intervening polymer chains is poorer, corresponding to a loss of excess (interaction) entropy. This is a well-known effect associated with both local length scales (as in atomic and for small molecule fluids[34,35]) and macromolecular (R_g) scales due to the long-range correlation hole effect.[32,37] (ii) A consequence of point i is reduced interfacial cohesion or poorer enthalpy associated with polymer−particle attractions. These two effects act in concert to enhance the repulsive barriers with increasing particle size and/or particle−polymer attraction strength.

Ultimately, the net result of all the above effects is a tendency of lower α value systems to have stronger, but fewer, locally stable bridging configurations. In contrast, increasing α leads to weaker, but more numerous, locally stable bridging states. It is conceivable that certain material combinations may result in a PMF with multiple, nearly equally probable local bridging configurations.

B. Particle Size Effects and Scaling Behavior. Our prior studies[17] of athermal polymer−particle mixtures discovered that for $D/d > 5-6$ there is a remarkably simple linear scaling behavior of the PMF with size ratio D/d. This critical value of D/d required for good collapse of $W_{cc}(r)$ appears to be determined by when the particle diameter exceeds the range of correlated (oscillatory) polymer density fluctuations ξ_ρ.[33] This known behavior motivates examination of a scaled PMF defined as $\bar{W}_{cc} \equiv W_{cc}d/D = f(\alpha,\epsilon_{pc})$, which may be a function only of the polymer−particle attraction strength and range.

Results typical of a large number of calculations are shown in Figure 5. Excellent collapse of the PMF occurs with deviations being a weak function of α and ϵ_{pc}. For $\alpha = 0.25$ (Figure 5a) this normalization yields good collapse for $D/d \geq 4$, However, for the corresponding $\alpha = 1$ sterically stabilized systems (inset of Figure 5a) good scaling occurs only for $D/d \geq 10$. Given the "bound layers" on each particle are ∼2−3 monomer diameters thick, the requirement of larger particles for the emergence of a universal scaling behavior is not unexpected. The existence of excellent master curves permits the depth and height of minima and maxima of the PMF for disparate particle sizes to be easily deduced. For example, for $\alpha = 0.25$ and assuming a 1 nm polymer segment size, a 30 nm particle has a $\sim 12k_BT$ bridging attraction when particle surfaces are separated a distance d. On the other hand, for the corresponding sterically stabilized system the effective repulsion between particles is roughly $150k_BT$ at contact.

Figure 5b shows analogous scaled PMF results for the $\alpha = 0.5$ system at both high (2.5, main panel) and moderate (1.0, inset) values of monomer−particle attraction. The collapse behavior of the $\alpha = 0.5$ system is generally very good. For $\epsilon_{pc} = 2.5$ there are visible deviations for the smallest particle diameter ($D/d = 4$),

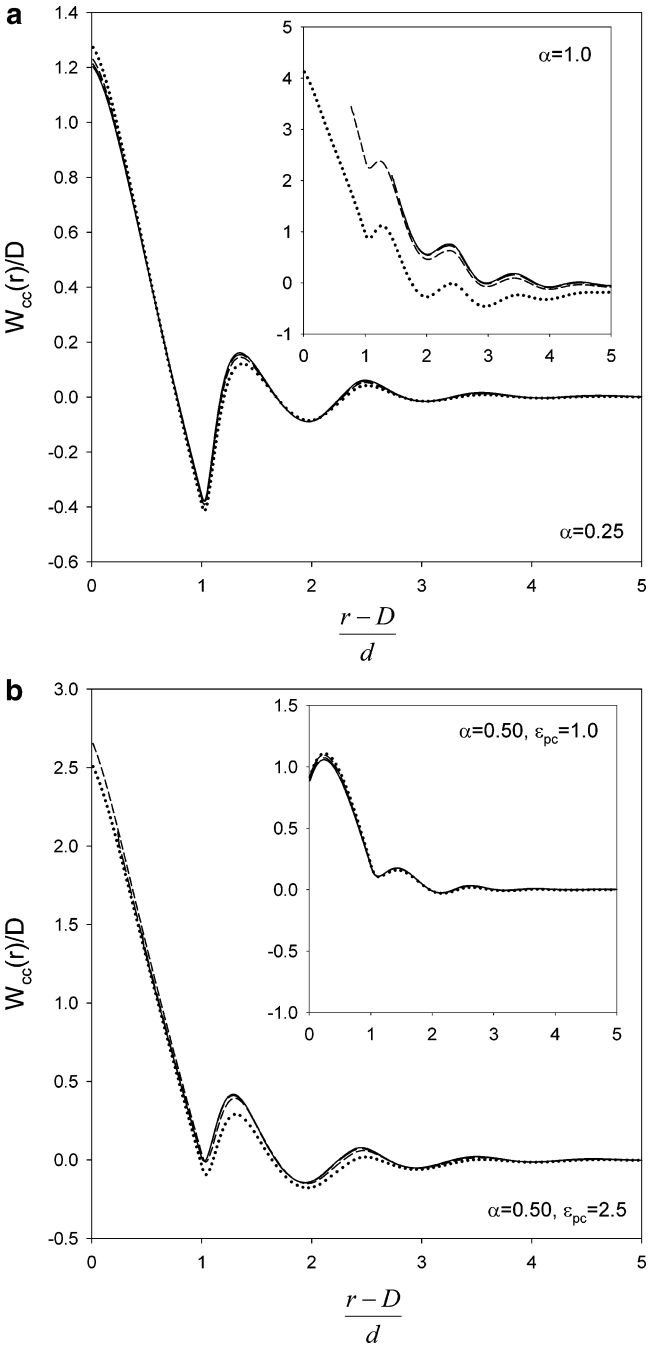

Figure 5. (a) Reduced potential of mean force, $\bar{W}_{cc} = W_{cc}d/D$, for systems with $\epsilon_{pc} = 2.5$ and $D/d = 4$ (dotted), 10 (short dash), 16 (long dash), and 24 (solid) for $\alpha = 0.25$ and $\alpha = 1.0$ (inset). (b) Reduced potential of mean force, $\bar{W}_{cc} = W_{cc}d/D$, for systems with $\alpha = 0.5$ and $D/d = 4$ (dotted), 10 (short dash), 16 (long dash), and 24 (solid) for $\epsilon_{pc} = 2.5$ and $\epsilon_{pc} = 1.0$ (inset).

which is likely due to this system being in a "crossover" regime in the sense it shows both bridging and steric stabilization features. Repulsive steric stabilization is dominant for $\epsilon_{pc} = 1.0$, while at $\epsilon_{pc} = 2.5$ the PMF is oscillatory with attractive and repulsive features including a $\sim 4.5k_BT$ bridging attraction at a separation distance of $2d$.

C. Local Structure−Interfacial Cohesion Relationships. On the basis of the size ratio scaled potentials of mean force, generic trends for the length scale and cohesion strength of the *most probable* interparticle separation can be identified. Figure 6a shows the reduced absolute magnitude of the deepest attractive

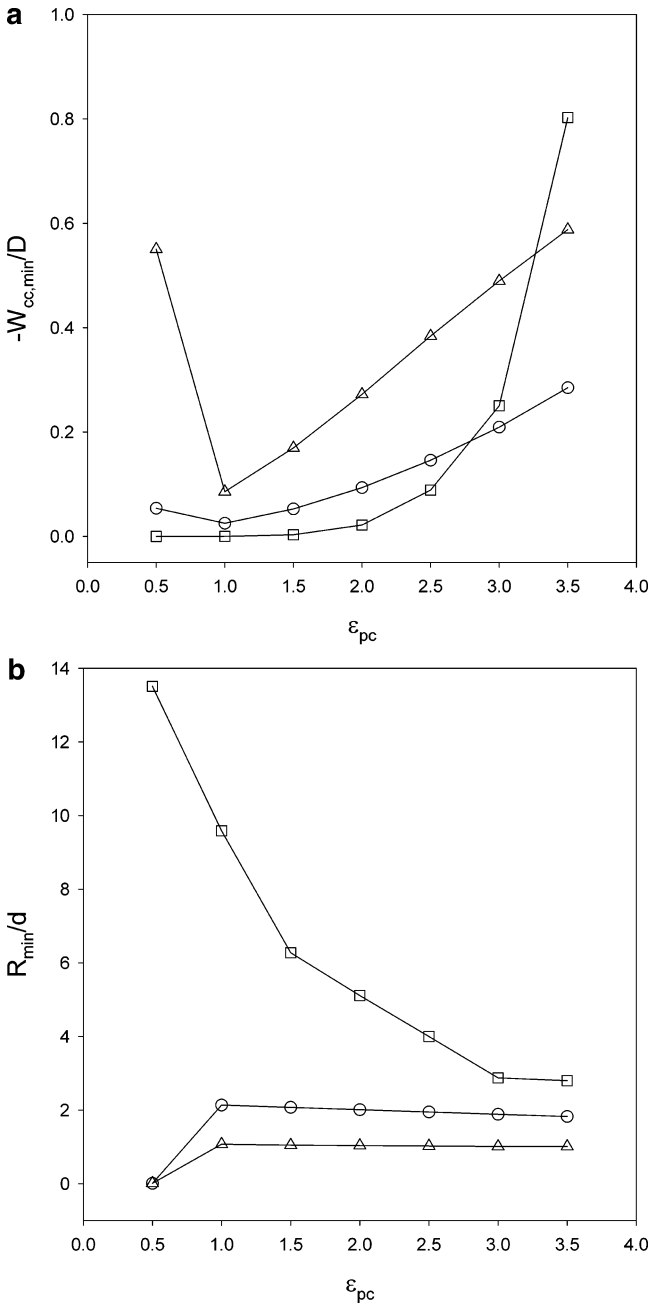

Figure 6. (a) Absolute magnitude of the global minimum of $\bar{W}_{cc}$ as a function of ϵ_{pc} for $\alpha = 0.25$ (triangles), 0.5 (circles), and 1.0 (squares). (b) Surface-to-surface interparticle separation, R_{min}, at the global minimum of $\bar{W}_{cc}$ as a function of ϵ_{pc} for $\alpha = 0.25$ (triangles), 0.5 (circles), and 1.0 (squares).

bridging well, $-\bar{W}_{cc,min}$, as a function of polymer−particle attraction strength for the three spatial ranges. For purely repulsive PMF's a value of zero is assigned to $-\bar{W}_{cc,min}$. In the limit of very small ϵ_{pc}, effectively athermal behavior occurs characterized by a very deep minimum of the PMF at contact (not shown). For the purpose of subsequent discussion we note that empirical experimental observations,[1,13] and also ideal dynamic mode coupling theory,[41,43] suggest the "rule of thumb" for particle gelation as when $-\bar{W}_{cc,min} \sim 3-4k_BT$. Figure 6b quantifies the corresponding interparticle separation at maximum attraction as a function of polymer−particle interaction strength and spatial range.

There are several notable trends in Figure 6a,b which, along with the results in Figures 3−5, form the basis of the summary of possible behavior in Figure 1. (i) For low ϵ_{pc} ($\epsilon_{pc} \leq 0.5$, dependent upon the value of α), the minimal value of $\bar{W}_{cc}(r)$ corresponds to contact entropic depletion attraction which deepens very rapidly as $\epsilon_{pc} \rightarrow 0$.[17] (ii) Beyond a moderate value ϵ_{pc}, the organization switches to bridging attraction or steric stabilization. In this regime of moderate polymer−particle attraction $-\bar{W}_{cc,min}$ increases as α decreases, highlighting the importance of bridging in localizing the particles. For the steric stabilization case ($\alpha = 1$) the attractive minima are very shallow. (iii) At high interfacial attraction ($\epsilon_{pc} \geq 3.0$), an interesting inversion of behavior occurs wherein the sterically stabilized scenario abruptly switches to a very strong bridging type behavior. The underlying physics for this process is not deeply understood. The pair correlations suggest that it may be related to the soft polymer layer surrounding the sterically stabilized particle reaching an effective "maximum packing" threshold, which would then imply a transition toward more hard-sphere-like behavior of the entire particle/bound layer unit. Note the optimum separation of particles in this limit is a bit larger than 3 monomer diameters (Figure 6b). (iv) For all the tight bridging cases, once contact aggregation is precluded ($\epsilon_{pc} > 0.5$) the location of the minimum remains fixed with increasing attraction strength. In contrast, the sterically stabilized particles show a continuous compression of the optimum interparticle spacing polymer layer as a function of increasing ϵ_{pc} until ultimately saturating at high interfacial attraction ($\epsilon_{pc} \approx 3.0-3.5$). For all cases the limiting, large ϵ_{pc} location of the minimum is directly related to the spatial range of the attraction. As α increases, the maximal bridging location changes in discrete units of a monomer diameter. (v) For all $\epsilon_{pc} > 1$ cases, the bridging attraction increases with polymer−particle attraction, roughly linearly for the shortest range interaction, moderately nonlinearly for the intermediate case ($\alpha = 0.5$), and extremely nonlinearly in a "threshold" type fashion for the longest range system. Note from Figures 4 and 5 that as the depth of the PMF increases at a given local minimum, the activation energy necessary for transitions between nearby local minima grows more rapidly than the well depth.

D. Effective Diameters in Sterically Stabilized Systems. The sterically stabilized behavior corresponds to purely repulsive interactions between particles and hence excellent dispersion of fillers in the polymer matrix. Since each particle has a thermodynamically stable "bound layer" of a few monomers thick, it is of interest to quantify an "effective diameter" of such repulsive entities. In analogy with charged colloids in solution,[1] an effective diameter $D_{eff} > D$ implies an effective particle volume fraction:

$$\phi_{eff} = \left(\frac{D_{eff}}{D}\right)^3 \phi \equiv \lambda^3 \phi \tag{18}$$

where λ^3 is the volume fraction amplification factor. When the effective packing fraction exceeds ~0.5 in charged colloidal suspensions, crystallization is often observed despite the low physical volume fraction.[1] Such an interesting phenomenon may be possible in polymer nanocomposites, i.e., crystalline type organization of fillers in a homopolymer matrix. To crudely investigate this possibility, we have computed an effective diameter based on the standard definition as the interparticle

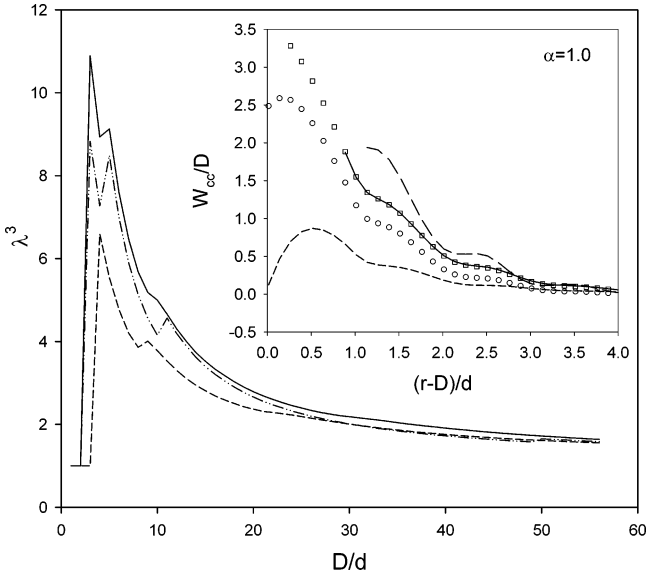

Figure 7. Effective volume fraction amplification factor (λ^3) of $\alpha = 1$ sterically stabilized particles for $\epsilon_{pc} = 0.25$ (dashes), $\epsilon_{pc} = 1.00$ (solid), and $\epsilon_{pc} = 1.75$ (dash−dot-dot). The inset shows the reduced PMF for representative examples in the sterically stabilized regime. At constant attraction ($\epsilon_{pc} = 1$) for $D = 4$ (circles), $D = 10$ (squares), and $D = 16$ (solid line) and at constant diameter $D = 16$ for $\epsilon_{pc} = 0.25$ (short dash), $\epsilon_{pc} = 1$ (solid), and $\epsilon_{pc} = 1.75$ (long dash).

separation where the effective repulsion equals the thermal energy:

$$W_{cc}(r = D_{eff}) = k_B T \tag{19}$$

Representative results for the volume fraction amplification factor are shown in Figure 7. For $D/d > 16$, the PMF master curves are employed, while for smaller values of D/d separate calculations have been performed. The "jaggedness" of the curves appears to be real and associated with monomer scale packing effects important for relatively small particles. Since the bound polymer layers are of an intrinsic thickness, the amplification factor must approach unity for large particles. For small enough particles, the PMF shows large deviations from the master curve. Their low surface area and large radius of curvature preclude the formation of dense adsorbed layers and efficient steric stabilization (see inset of Figure 7). Hence, λ decreases and approaches unity in the very small particle limit. This implies there is an optimum intermediate *nano*particle size for which the effective volume fraction is maximum, which we estimate from Figure 7 as ∼5−6 monomer diameters (∼3−6 nm). The amplification factor also depends on the strength of the polymer−particle attraction in an interesting nonmonotonic manner, first increasing and then decreasing with ϵ_{pc}. The former trend is a consequence of denser adsorbed layers with increasing polymer−particle attraction. The latter trend is a precursor of the qualitative change in the PMF from steric stabilization to "tele-bridging" discussed above (see Figures 1 and 6).

The maximum amplification factor is ∼6−10. Using a particle packing fraction of ∼0.5 as a crude metric for crystallization, and the total packing fraction of 0.4 of our present calculations suggests crystallization might be possible for physical volume fraction of 10% or so.

IV. Role of Polymer Degree of Polymerization

For sufficiently large size asymmetry ratios ($D/d >$ 4−6) in dense melts the various modes of equilibrium *local* particle organization (depletion attraction, steric stabilization, bridging) are not fundamentally polymeric phenomena. That is, the effect of degree of polymerization is expected to be of a quantitative nature, to a degree that may depend on the mode of organization. To explore this issue, we have performed PMF calculations over a wide range of $N = 25-1600$. Calculations have been done at both (nominally) fixed monomer packing fraction and for the more experimentally realistic situation[32] of fixed polymer melt dimensionless compressibility ($S_{pp}(k = 0) =$ constant).

A. Local Structure. The main frame of Figure 8a shows iso-$S_{pp}(0)$ results for $\alpha = 1$ and a strong polymer−particle attraction of $3k_BT$. Recall this is the situation of longer range bridging (see Figure 6) which should magnify any polymer chain length effects. The local (monomer scale) attractive minima of the PMF at larger separations are only slightly sensitive to chain length. The minimum at $r - D = 2d$ is monotonically destabilized with increasing N. All repulsive barriers are strongly enhanced with increasing degree of polymerization. Hence, at very small interparticle separations, and also at unfavorable separations corresponding to maxima of the PMF, we find that increasing chain length results in enhanced polymer-mediated repulsion between particles. This is a consequence of the two physical effects (packing entropy and interfacial enthalpy) discussed at the end of section IIIA.

Figure 8b shows analogous results for the intermediate range ($\alpha = 0.5$) polymer−particle attraction (main panel) where strong and tight bridging occurs. The trends are qualitatively the same as in Figure 8a. However, the small effect of N on the global minimum (here at $r - D \sim 2d$) is reversed, with longer chains providing a bit more cohesion in the bridging configuration. Physically this might be interpreted as a geometric consequence of longer chains being able to better "bridge" the curved surfaces of particles.

The inset of Figure 8b shows results for $\alpha = 1$ and a weaker interfacial attraction corresponding to steric stabilization behavior. An increase of polymer chain length monotonically increases the interparticle repulsion. In essence, the bound layers are more effective at pushing the particles apart, a trend which seems physically intuitive. Note that in all cases in Figure 8 as particles are pushed into close contact strong repulsions emerge which are enhanced for longer chains.

The N-dependent trends in the mainframe of Figure 8a are qualitatively reversed if the calculations are performed at fixed polymer packing fraction (inset of Figure 8a). This is related to the well-known and understood problem that ideal chain models have an increasing intramolecular overlap with increasing N (ultimately saturating in the long chain limit).[32] This translates to a smaller effective packing fraction and a higher compressibility.[32] The iso-$S_{pp}(0)$ calculations attempt to correct this deficiency in an experimentally motivated manner since the bulk modulus of polymer melts at fixed temperature and pressure is nearly N-independent.[44] For the systems in Figure 8b, calculations based on nominally constant packing fraction (not shown) are qualitatively the same as the isocompressibility results but the N-dependent trends are significantly exaggerated.

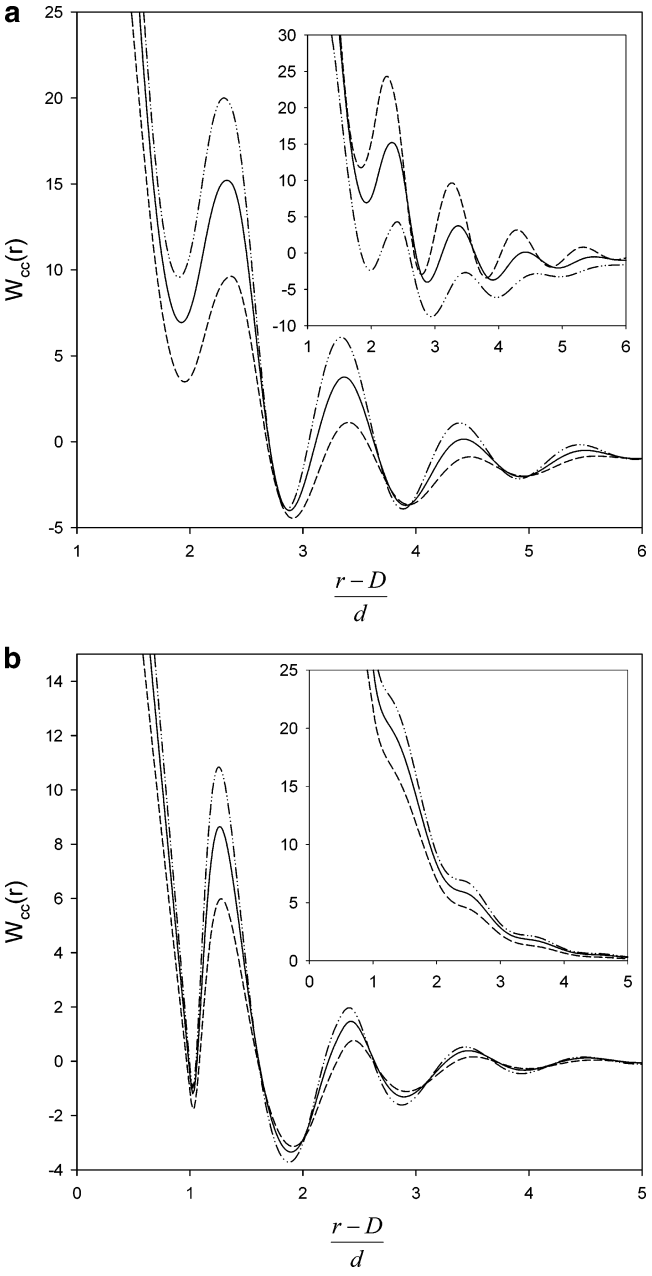

Figure 8. (a) Dependence on chain length of the PMF for $D = 16$, $\alpha = 1.0$, and $\epsilon_{pc} = 3.0$ for both the compressibility adjusted and nonadjusted (inset) systems for $N = 25$ (dashed), $N = 100$ (solid), and $N = 1600$ (dash−dot−dot). The reference compressibility was matched to the $N = 100$ system. (b) compressibility adjusted PMF for $D = 8$, $\alpha = 0.5$ ($\alpha = 1.0$), and $\epsilon_{pc} = 3.0$ ($\epsilon_{pc} = 1.0$) is plotted in the main (inset) graph for $N = 25$ (dashed curve), 100 (solid curve), and 1600 (dash−dot curve).

B. Long-Range Effects. A unique feature of high polymers is the existence of a universal long-range part of their intermonomer pair correlations known as the "correlation hole".[32,45] Because of the combined constraints of chain connectivity and uncrossability, intermolecular pair correlations do not randomize until monomers are separated a distance of order the coil radius of gyration $R_g \propto \sqrt{N}\, d$. Such a correlation effect could mediate a component of the particle PMF of an amplitude and spatial range controlled by the radius of gyration length scale. Alternatively, for the problem of polymer melts between two flat surfaces it is generally believed that because the polymer density−density

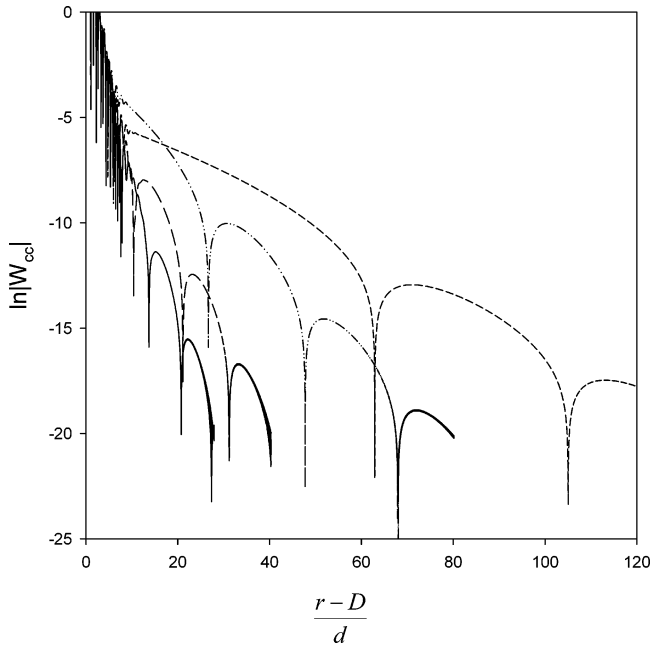

Figure 9. Natural log−linear plot of the isocompressibility PMF over a wide range of amplitudes and interparticle separations for $D = 16$, $\alpha = 1.0$, $\epsilon_{pc} = 3.0$, and $N = 50$ (solid), $N = 100$ (long dash), $N = 400$ (dash−dot−dot), and $N = 1600$ (short dash). The $N = 100$ chain is taken as the basis for the correction of compressibility.

fluctuation correlation length is an intrinsic length scale essentially independent of macromolecular size, there is no long-range component of surface forces.[28,46] Since particles are curved objects of finite size, it is not obvious this argument for surfaces applies.

Representative calculations that address the macromolecular scale aspects of the PMF are shown in Figure 9 for a wide range of chain lengths from $N = 50-1600$. A logarithmic scale is employed since the PMF has a local part of large amplitude and a very weak long-range part. To zeroth order, we find the weak, long-range features are not sensitive to the details of the polymer−particle attractive potential, and hence results for a single choice of α and ϵ_{pc} are shown. On local scales, the interparticle PMF is oscillatory with a period of approximately d which reflects intermonomer packing correlations. The decay length or envelope of the local part of the PMF is determined by the correlation length of collective density fluctuations of the pure polymer melt ("mesh size")[33] and is insensitive to N. As the particles become widely separated (roughly $>4-6d$), these local correlations become exponentially small, and a long-range component of the PMF emerges characterized by an amplitude and spatial range controlled by R_g. This macromolecular scaling implies the origin of the weak long-range feature is the correlation hole effect. There are secondary dependences on the details of the polymer−particle attractions (not plotted). For example, for small α the transition between the local and macromolecular regimes occurs sharply, while for larger α there is a discernible intermediate crossover regime of width controlled by both α and ϵ_{pc}.

The scaling of the long-range features of the PMF might be reminiscent of a polymer bridging mechanism that readily occurs in solution,[13] but its relative strength is extremely weak in low compressibility melts. Thus, while such long-range effects are not perfectly "screened out", they are nearly so and presumably have little practical consequences.

V. Sticky Fillers: Effect of Direct Particle Attractions

Real fillers dissolved in solution or a polymer matrix interact through unbalanced van der Waals attractions. As is well-known in colloid science,[1] the magnitude of such a *net* attraction is controlled by chemical differences (e.g., dielectric constant mismatch) between the particles and "solvent", which in the present case are polymers. For example, carbon-based fillers dissolved in hydrocarbon polymers (or silica fillers in siloxane polymers) will experience significantly weaker dispersion attractions than silica fillers in a hydrocarbon polymer matrix. The strength of attraction also scales with the particle diameter and is typically of a "short" nanometer scale range controlled by the size of the elementary constituents of the particle (i.e., the parameter b in section IIB). As discussed in section IIB, the energy of two fillers at contact is given by $U_{cc}(r = D) = -\epsilon_{cc} = -E_{cc}(D/4b)$, with the attractive branch of the CLJ potential shifted so it coincides with the particle−particle distance of closest approach. Here, as elsewhere, all energies are reported in thermal energy units. In this section we use the CLJ potential to study how the direct van der Waals attractions compete with the polymer-mediated part of the PMF. In the dilute two-particle limit the total particle PMF is simply the sum of the polymer-mediated part studied in section III and the direct contribution, i.e., $W_{cc}(r) + U_{cc}(r)$. The values of ϵ_{cc} are chosen so that they correspond to weak, comparable, or stronger attractions than the interfacial attraction strength as quantified by ϵ_{pc} in eq 11. Outside the very small particle regime, both the direct van der Waals and polymer-induced contributions to the total PMF scale with particle diameter D. Hence, to a good first approximation one can address the competition between the two distinct contributions to the PMF in a size ratio independent manner by studying $(W_{cc}(r) + U_{cc}(r))(d/D)$. Representative results for this quantity are shown in Figure 10 for $D/d = 16$, $d/b = 3$, and three values of the polymer−particle attraction range.

Figure 10a shows results for the shortest range ($\alpha = 0.25$) case for $\epsilon_{cc} = (0.5,1.0)\epsilon_{pc}$ with $\epsilon_{pc} = 3$ (main frame) and $\epsilon_{pc} = 1$ (inset). For weaker particle−polymer interfacial cohesion, the direct interparticle attraction results in a potential of mean force which rapidly shifts from bridging behavior with contact aggregation energetically and kinetically (barrier) disfavored to a state where direct contact aggregation of nanoparticles is favored. For the large interfacial attraction system ($\epsilon_{pc} = 3.0$) a similar sequence of changes occur with increasing direct van der Waals attraction, although comparable energetics ($\epsilon_{cc} = \epsilon_{pc}$) are required to stabilize the contact aggregation state. Figure 10b,c shows results for the other two values of α and a wider range of direct interparticle attraction of $\epsilon_{cc} = (1,3)\epsilon_{pc}$. For the $\alpha = 0.5$ system the longer spatial range of the interfacial attraction contributes a significant amount of stabilization. At low values of interfacial attraction the particle organization can be tuned from dispersed ($\epsilon_{cc} = 0$) to aggregated ($\epsilon_{cc} = 3\epsilon_{pc}$) for weak ($\epsilon_{pc} = 1$) interfacial attraction or from bridging to contact aggregation for higher interfacial attraction, including reorganization of the preferred bridging distance. Because of the presence of both bridging and steric stabilization behavior in the hard filler PMF for $\alpha = 0.5$, the direct van der Waals attraction can shift the interparticle bridging separation to smaller distances while maintaining the

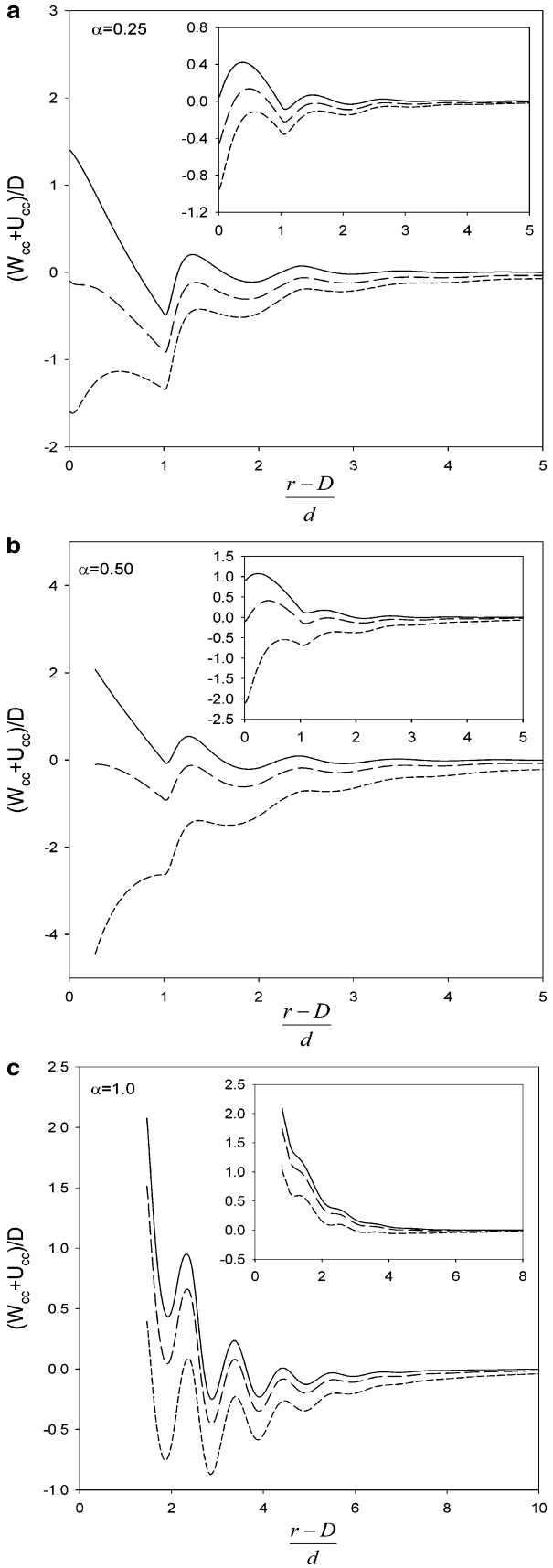

Figure 10. Total PMF divided by D/d for three interfacial plus direct interparticle van der Waals attraction systems with $D/d = 16$ and $\epsilon_{pc} = 3.0$ ($\epsilon_{pc} = 1.0$) in the main (inset) panel and (a) $\alpha = 0.25$ and $\epsilon_{cc}/\epsilon_{pc} = 0$ (solid), 0.5 (long dash), and 1.0 (short dash), (b) $\alpha = 0.50$ and $\epsilon_{cc}/\epsilon_{pc} = 0$ (solid), 1.0 (long dash), and 3.0 (short dash), and (c) $\alpha = 1.0$ and $\epsilon_{cc}/\epsilon_{pc} = 0$ (solid), 1.0 (long dash), and 3.0 (short dash).

basic bridging structure, unlike the complete destruction of bridging in favor of aggregation observed for $\alpha = 0.25$. Of course, sufficient increase of ϵ_{cc} ultimately destroys bridging entirely, resulting in strong contact aggregation.

Figure 10c shows that increasing the particle−polymer attraction range further ($\alpha = 1.0$) results in PMF shapes that are not strongly perturbed by direct van der Waals interactions even when very strong ($\epsilon_{cc} = 3\epsilon_{pc}$). The reason is that the large α system is strongly sterically stabilized by bound polymer layers, especially if the interfacial attraction is relatively weak. For large interfacial attraction recall there is a crossover to a strong, but more long range, "tele-bridging" type of organization. Direct attraction serves to amplify the attractive features of the PMF for hard fillers and results in the emergence of many (four in Figure 10c) attraction wells of significant depth.

VI. Discussion and Summary

A systematic PRISM theory study has been performed to determine the potential of mean force between a pair of spherical particles dissolved in a dense homopolymer melt. The role of particle-to-monomer size ratio (D/d), degree of polymerization (N), strength (ϵ_{pc}), and spatial range (αd) of monomer−particle attractions and direct interfiller van der Waals attractions has been established. For roughly $D/d > 6$, the potential of mean force scales linearly with D/d. This allows the construction of "master curves" and the quantification of the material-specific aspects independent of the relative filler/monomer diameter ratio.

For hard-sphere fillers, four general categories of behavior or scenarios are found which are summarized at the cartoon level in Figure 1. At low enough interfacial energy, all systems behave in an essentially athermal manner, with direct nanoparticle aggregation (case (i)) due to the extremely large depletion attraction between the particles. As ϵ_{pc} increases, the depletion attraction lessens due to competition from, and eventual domination by, the enthalpy gain of polymer segments adsorbing onto the particle surface. In general, all systems exhibit attractive wells ($W_{cc}(r) < 0$) at some threshold value of ϵ_{pc}, beyond which particles tend to localize at system-specific separations. For low and moderate values of α at all ϵ_{pc}, the particles are bridged (case (iii)) at a distance of nd, where n is a quantized function of α and generally ranges from 1 to 4. For larger α, at low ϵ_{pc} the nanoparticles are sterically stabilized with thermodynamically stable adsorbed layers of polymer acting as cushions between the particles (case (ii)); at higher ϵ_{pc} a bridging-type attraction emerges on top of the already established steric stabilization layer (case (iv)). The latter behavior is called a "tele-bridged" configuration which has similiarities to bridging in low-α systems but at larger distances associated with a (sterically stabilized) effective particle radius. Although very computationally intensive, computer simulations should be able to critically test these theoretical results for particles and polymers of modest sizes.

Our results also have implications for nonequilibrium phenomena. The most obvious is polymer-mediated gelation or filler network formation which can be crudely identified with the emergence of a minimum in the PMF deeper than roughly $3-4k_BT$. Such minima can occur at contact or separated by variable discrete multiples of the monomer diameter depending on system parameters. The repulsive barriers that separate local minina are also relevant in practice since they may or may not be surmountable in any reasonable amount of time. Barriers can result in kinetic stabilization against aggregation or simply restrict access to the tightest and most cohesive interparticle separations in the PMF.

Direct interparticle van der Waals interactions favor contact aggregation and hence compete with the rich polymer-mediated behavior in their absence. As they increase in strength, bridging configurations are gradually destabilized and replaced with contact aggregation as the most favored state. However, noncontact bridging minima often survive as metastable local minima, which may be significantly populated for either equilibrium or kinetic reasons due to the presence of barriers. Steric stabilization systems are much less perturbed by direct van der Waals attractions due to the thermodynamic stability of two distinct "bound layers" which resist interpenetration or desorption. This raises the interesting experimental possibility of tuning the interfacial strength and spatial range to achieve miscibility and good particle dispersion in real polymer nanocomposites. In addition, when the net PMF is purely repulsive, there may be the possibility of crystallizing nanoparticles in the polymer matrix at relatively low loadings. The physics is analogous to charged colloidal suspensions,[1] where now the effective diameter of particles is strongly enhanced by the "bound" polymer layers, and hence an effective volume fraction can be much larger than the physical volume fraction.

The effect of polymer degree of polymerization is relatively weak. This is to be expected in equilibrium under dense melt conditions where the collective polymer melt density fluctuation correlation length is of the order of a monomer diameter.[33] Varying N can fine-tune the PMF, enhance or suppress local minimum features, and significantly modify local barrier heights, aspects which can have important consequences in practice. A long-range and very weak feature in the PMF has also been found. Its amplitude and range are controlled by the polymer radius of gyration and are identified with the incompletely screened consequences of the polymer correlation hole effect on the interparticle PMF. There is theoretical precedence for a long-range part of $g_{cc}(r)$ in polymer−colloid suspensions.[3] However, from a practical perspective this contribution to the PMF is so weak (generally $\ll k_BT$) under nearly incompressible melt conditions that it likely has negligible consequences.

The present work has focused on the elementary problem of two spherical fillers dissolved in a freely jointed chain polymer melt. There are many future directions to pursue. The most obvious is mixtures at finite particle volume fractions. Many-body effects will be important, polymer matrix correlations will be perturbed, and distinctive signatures of the state of organization will be encoded in the collective partial scattering structure factors which are potentially amenable to measurement using X-ray or neutron scattering. Some of the more detailed trends for the two particle potential of mean force may be modified due to such many particle packing effects and interference between polymer organization around different particle pairs. How to tune material parameters to achieve thermodynamically miscible polymer nanocomposites is a problem of major materials importance and can be studied. The issue of particle-induced changes in poly-

mer conformation is also relevant and can be treated using the more computationally demanding fully self-consistent version of PRISM theory.[32] Nonspherical fillers, such as nanorods, carbon nanotubes, or clay disks, are also of great interest and can be studied using PRISM theory.[47,48] Systems where polymers are grafted to the particle surfaces and then dissolved in homopolymer matrices are of fundamental and practical importance, and connections to spherical micelle forming diblock copolymers, many-arm stars, and soft colloidal fluids are likely. Finally, much of the interest in polymer nanocomposites involves mechanical property modification such as shifts in the glass transition temperature and strongly modified viscoelastic response.[9,11,49−54] Our present results provide potentially important structural input to modern statistical dynamical theories, such as mode coupling[41−43] and beyond[55,56] approaches, which may allow the prediction of both a network formation transition and viscoelastic properties. Work in many of the above directions is ongoing.

Acknowledgment. This work was supported by the Nanoscale Science and Engineering Initiative of the National Science Foundation under NSF Award DMR-0117792 and Oak Ridge National Laboratory via the Division of Materials Science of the Department of Energy. Discussions and/or correspondence with P. Keblinski, S. K. Kumar, S. Q. Wang, and S. Egorev are gratefully acknowledged.

References and Notes

(1) Russel, W. B.; Saville, D. A.; Schowalter, W. R. In *Colloidal Dispersions*; Cambridge University Press: Cambridge, 1989.
(2) Poon, W. C. K. *J. Phys.: Condens. Matter* **2002**, *14*, R859.
(3) Fuchs, M.; Schweizer, K. S. *J. Phys.: Condens. Matter* **2002**, *14,* R239.
(4) Ramakrishnan, S.; Zukoski, C. F. In *Dekker Encyclopedia of Nanoscience and Technology*; Schwarz, J. A., Contescu, C. I., Putyera, K., Eds.; Marcel Dekker: New York, 2004; p 2813.
(5) Wang, M.-J. *Rubber Chem. Technol.* **1998**, *71*, 520; **1999**, *72*, 430.
(6) Huber, G.; Vilgis, T. A. *Macromolecules* **2002**, *35*, 9204.
(7) Vieweg, S.; Unger, R.; Heinrick, G.; Donth, E. *J. Appl. Polym. Sci.* **1999**, *73*, 495.
(8) Ajayan, P. M.; Schadler, L. S.; Braun, P. V. *Nanocomposite Science and Technology;* KGaA: Weinheim, 2003; p 77.
(9) Ash, B. J.; Schadler, L. S.; Siegel, R. W. *Mater. Lett.* **2002**, *55*, 83.
(10) Lin, Y.; Boker, A.; He, J.; Sill, K.; Xiang, H.; Abetz, C.; Li, X.; Wang, J.; Emrick, T.; Long, S.; Want, Q.; Balazs, A.; Russell, T. P. *Nature (London)* **2005**, *434*, 55.
(11) Mackay, M. E.; Dao, T. T.; Tuteja, A.; Ho, D. L.; Van Horn, B.; Kim, H.-C.; Hawker, C. J. *Nature (London) Mater*. **2003**, *2*, 762.
(12) Ellise, R. J.; Minton, A. P. *Nature (London)* **2003**, *425*, 27.
(13) Larson, R. G. *The Structure and Rheology of Complex Fluids*; Oxford University Press: New York, 1999.
(14) Yethiraj, A. *Adv. Chem. Phys.* **2002**, *121*, 89.
(15) Yethiraj, A.; Hall, C. K. *J. Chem. Phys.* **1991**, *95*, 3749.
(16) Patel, N.; Egorov, S. A. *J. Chem. Phys.* **2004**, *121*, 4987.
(17) Hooper, J. B.; Schweizer, K. S.; Desai, T. G.; Koshy, R.; Keblinski, P. *J. Chem. Phys.* **2004**, *121*, 6986.
(18) Salaniwal, S.; Kumar, S. K.; Douglas, J. F. *Phys. Rev. Lett.* **2002**, *89*, 258301.
(19) Starr, F. W.; Schroeder, T. B.; Glotzer, S. C. *Macromolecules* **2002**, *35*, 4481; *Phys. Rev. E* **2001**, *64*, 021802.
(20) Starr, F. W.; Douglas, J. F. *J. Chem. Phys.* **2003**, *119*, 1777.
(21) Vacatello, M. *Macromolecules* **2001**, *34*, 1946; **2002**, *35*, 8191.
(22) Doxastakis, M.; Chen, Y. L.; Guzman, O.; dePablo, J. J. *J. Chem. Phys.* **2004**, *120*, 9335.
(23) Smith, J. S.; Bedrov, D.; Smith, G. D. *Compos. Sci. Technol.* **2003**, *63*, 1599.
(24) Bedrov, D.; Smith, G. D.; Smith, J. S. *J. Chem. Phys.* **2003**, *119*, 10438.
(25) Yethiraj, A.; Hall, C. K.; Dickmam, R. *J. Colloid Interface Sci.* **1992**, *151*, 102.
(26) Dickman, R.; Yethiraj, A. *J. Chem. Phys.* **1994**, *100*, 4683.
(27) Khalatur, P. G.; Zherenkova, L.; Khoklov, A. R. *Physica A* **1997**, *247*, 205.
(28) Joanny, J. F.; Leibler, L.; deGennes, P. G. *J. Polym. Sci., Polym. Phys.* **1979**, *17*, 1073.
(29) Scheutjens, J. M. H. M.; Fleer, G. J. *Adv. Colloid Interface Sci.* **1982**, *16*, 361.
(30) Eisenriegler, E. *J. Chem. Phys.* **2000**, *113*, 5091; *Phys. Rev. E* **1997**, *55*, 3116.
(31) Odijk, T. *J. Chem. Phys.* **1997**, *106*, 3402.
(32) Schweizer, K. S.; Curro, J. G. *Adv. Chem. Phys.* **1997**, *98*, 1.
(33) Koshy, R.; Desai, T. G.; Keblinski, P.; Hooper, J.; Schweizer, K. S. *J. Chem. Phys.* **2003**, *119*, 7599.
(34) Chandler, D.; Andersen, H. C. *J. Chem. Phys.* **1972**, *57*, 1930. Chandler, D. In *Studies in Statistical Mechanics VIII*; Montroll, E. W., Lebowitz, J. L., Eds.; North-Holland: Amsterdam, 1982; p 274.
(35) Hansen, J. P.; McDonald, I. R. *Theory of Simple Liquids;* Academic Press: London, 1986.
(36) Henderson, D.; Duh, D. M.; Chu, X.; Wasan, D. *J. Colloid Interface Sci.* **1997**, *185*, 265.
(37) Doi, M.; Edwards, S. F. *Theory of Polymer Dynamics*; Oxford University Press: New York, 1986.
(38) Kremer, K.; Grest, G. S. *J. Chem. Phys.* **1990**, *92*, 5057.
(39) Fuchs, M.; Schweizer, K. S. *Europhys. Lett.* **2000**, *51*, 621; *Phys. Rev. E* **2001**, *64*, 021514.
(40) Bicerano, J. *Prediction of Polymer Properties*; Marcel Dekker: New York, 1993.
(41) Götze, W. *J. Phys.: Condens. Matter* **1999**, *11*, A1. Götze, W.; Sjogren, L. *Rep. Prog. Phys.* **1992**, *55*, 241.
(42) Bergenholtz, J.; Poon, W. C. K.; Fuchs, M. *Langmuir* **2003**, *19*, 4493. Bergenholtz, J.; Fuchs, M. *Phys. Rev. E* **1999**, *59*, 5706. Fabbian, L.; Götze, W.; Sciortino, F.; Tartaglia, P.; Thiery, F. *Phys. Rev. E* **1999**, *59*, R1347. Zaccarelli, E.; Foffi, G.; Dawson, K. A.; Sciortino, F.; Tartaglia, P. *Phys. Rev. E* **2001**, *63*, 031501.
(43) Chen, Y. L.; Schweizer, K. S. *J. Chem. Phys.* **2004**, *120*, 7212.
(44) . Schweizer, K. S.; Curro, J. G. *J. Chem. Phys.* **1988**, *89*, 3350. Honnell, K. G.; Curro, J. G.; Schweizer, K. S. *Macromolecules* **1990**, *23*, 3496. In addition to experimental motivations, density functional theory (DFT) of pearl-necklace chains near a hard wall have shown that the correct specification of the system compressibility is necessary to capture the proper qualitative packing behavior of the monomers near the surface. See: Hooper, J. B.; Pileggi, M. T.; McCoy, J. D.; Curro, J. G.; Weinhold, J. D. *J. Chem. Phys.* **1999**, *112*, 3094.
(45) DeGennes, P. G. *Scaling Concepts in Polymer Physics*; Cornell University Press: Ithaca, NY, 1979.
(46) Israelachvili, J. *Intermolecular and Surface Forces*; Academic Press: London, 1997.
(47) Chen, Y. L.; Schweizer, K. S. *J. Chem. Phys.* **2002**, *117*, 1351; *Langmuir* **2002**, *18*, 7354.
(48) Harnau, L.; Costa, D.; Hansen, J. P. *Europhys. Lett.* **2001**, *53*, 729.
(49) Tsagaropoulos, G.; Eisenberg, A. *Macromolecules* **1995**, *28*, 6067.
(50) Ash, B. J.; Schadler, L. S.; Seigel, R. W. *J. Polym. Sci., Polym. Phys.* **2004**, *42*, 4371.
(51) Berriot, J.; Montes, H.; Lequeux, F.; Long, D.; Sotta, P. *Macromolecules* **2002**, *35*, 9756. Montes, H.; Lequeux, F.; Berriot, J. *Macromolecules* **2003**, *36*, 8107.
(52) McCoy, J. D.; Curro, J. G. *J. Chem. Phys.* **2002**, *116*, 9154.
(53) Sternstein, S. S.; Zhu, A. J. *Macromolecules* **2002**, *35*, 7262.
(54) Huber, G.; Vilgis, T. A. *Macromolecules* **2002**, *35*, 9204.
(55) Schweizer, K. S.; Saltzman, E. J. *J. Chem. Phys.* **2003**, *119*, 1181. Saltzman, E. J.; Schweizer, K. S. *J. Chem. Phys.* **2003**, *119*, 1197.
(56) Chen, Y. L.; Kobelev, V.; Schweizer, K. S. *Phys. Rev. E* **2005**, *71*, 041405.

MA051318K